IEEE Access
Multidisciplinary | Rapid Review | Open Access Journal

Received April 11, 2018, accepted May 14, 2018, date of publication May 31, 2018, date of current version July 12, 2018.

Digital Object Identifier 10.1109/ACCESS.2018.2838329

An Improved H/α Unsupervised Classification Method for Circular PolSAR Images

FEITENG XUE, (Student Member, IEEE), YUN LIN, (Member, IEEE), WEN HONG, (Member, IEEE), SHIQIANG CHEN, (Student Member, IEEE), AND WENJIE SHEN, (Student Member, IEEE)

Key Laboratory of Technology in Geospatial Information Processing and Application System, Institute of Electronics, Chinese Academy of Sciences, Beijing 100190, China
University of Chinese Academy of Science, Beijing 100190, China

Corresponding author: Wen Hong (whong@mail.ie.ac.cn)

This work was supported by the National Natural Science Foundation of China under Grants 61331017, 61431018, 61571421, 61571419, and 61501210.

ABSTRACT In conventional polarimetric synthetic aperture radar, targets are usually assumed isotropic, and potential polarimetric variations in azimuth are ignored. As to polarimetric circular SAR (CSAR), the azimuthal aperture is much larger, and polarimetric variations in azimuth are no longer negligible. Moreover, whether a target has changed polarimetric properties in azimuth, i.e., anisotropic, is an important feature. H/α classification scheme is a famous and effective unsupervised classification method. However, when applying H/α classification scheme against polarimetric CSAR data, problems occur. First, during the formation of a large aperture, polarimetric properties from different angles of view are combined, which affects the estimation of H and α. Second, H/α method cannot distinguish anisotropic and isotropic targets. In this paper, a pixel-wise H/α calculation method and an unsupervised classification scheme against polarimetric CSAR images are proposed to solve the two problems. With the pixel-wise H/α calculation method, H and α are more accurately calculated. Meanwhile, anisotropic and isotropic targets which have same scattering mechanism can be distinguished by the proposed classification method. The effectiveness of the pixel-wise H/α calculation method is demonstrated by both the simulated and real data. The unsupervised classification method is demonstrated based on real data, acquired by airborne CSAR system at P-band, the Institute of Electronics, Chinese Academy of Sciences, Beijing, China.

INDEX TERMS Anisotropic, circular SAR, entropy, polarimetry, unsupervised classification.

I. INTRODUCTION

In conventional polarimetric synthetic aperture radar (PolSAR), targets are usually assumed isotropic and potential polarimetric variations in azimuth are ignored. In some new synthetic aperture radar(SAR) modes, such as polarimetric circular SAR(CSAR), the azimuthal view angle is much larger and polarimetric variations in azimuth are no longer negligible. Moreover polarimetric variations should be viewed as important properties and can help researchers to achieve better understanding and more precise classification result of interesting targets. However traditional classification methods only use full aperture data and ignore the polarimetric variations in azimuth. Thus traditional classification methods can not be directly applied to polarimetric CSAR images. An improved classification method which uses polarimetric variations in azimuth as an important feature is needed.

With the development of PolSAR system which has large aperture and high resolution, anisotropic scatterings are studied by Ponce *et al.* [1], Lin *et al.* [2], Ferro-Famil *et al.* [3], Flake *et al.* [4], Runkle *et al.* [5], Zhao *et al.* 6], Xu *et al.* [7], Li *et al.* [8], and Moses *et al.* [9]. Anisotropic Bragg scattering in polarimetric wide-angle SAR, which is due to the coherent summation of simultaneously constructive contributions from a set of scatterers in agricultural areas, is analyzed with maximum likelihood ratio in [3]. Then in [10] polarimetric variations in azimuth are viewed as a part of targets' polarimetric properties and are used as features in polarimetric classification. In [7], a parameter is proposed to quantitatively describe anisotropy. In [11], multi-aperture polarimetric entropy(MAPE) is proposed to quantitatively describe both polarimetric variations in azimuth and polarimetric randomness.

H/α method is very successful in the polarimetric classification field. The method classifies polarimetric data based on polarimetric randomness, H and average polarimetric scattering, α [12]. As an unsupervised method, H/α method classifies polarimetric data into dihedral, dipole and Bragg scatterings which are of high concern by researchers in polarimetric field. Many classification methods based on H/α method are proposed [12]–[17]. In [16], H/α classification result is used as initial classification map. Then complex Wishart classifier is applied to achieve an improved classification result and better interpretation of each class. In [14], the classification of multi-frequency polarimetric data is discussed. The proposed method uses H/α classification result as initial data set. Then Maximum Likelihood decision rules and cross-correlation information between different frequencies are used to improve the classification result. However, when applying H/α method to polarimetric CSAR data, there are two problems. Firstly, during the formation of large aperture, polarimetric mechanisms from different angles of view are combined, which can affect the estimation of H and α. Secondly, anisotropic targets are defined as having dominant directions and different scattering mechanisms from different angles of view. The meaning of 'anisotropic' is different from parameter A(polarimetric anisotropy) in H/A/α decomposition since A mainly expresses the secondary scattering process. The scattering mechanisms of anisotropic targets are usually represented by scattering mechanisms from the dominant directions. Isotropic targets are defined as having same polarimetric mechanisms from different angles of view. Since H/α method uses only scattering mechanisms to classify targets, anisotropic and isotropic targets of same scattering mechanisms are hard to distinguish in H/α scheme.

In this paper, pixel-wise method to calculate H and α is proposed to avoid the affection of polarimetric variations in azimuth. Firstly, MAPE is used to identify anisotropic and isotropic targets. Then, the scattering directions of anisotropic targets are detected by maximum likelihood ratio. Consequently the corresponding sub-aperture is detected. Then data from the corresponding sub-aperture are used to calculate H and α. As to isotropic targets, H and α are calculated with full aperture data. The effectiveness of our proposed calculation method is demonstrated based on both simulated and real polarimetric CSAR data. An unsupervised classification method is then proposed. The method is based on MAPE and pixel-wise H/α. The proposed classification method uses MAPE as third dimension to classify data based on both polarimetric properties and polarimetric variations in azimuth. Then the method is further improved by reducing five classes and using only MAPE and pixel-wise α as classification features. The effectiveness of our proposed classification method is demonstrated based on real polarimetric CSAR data.

The remainder of this paper is organized as follows: Method to calculate pixel-wise H/α is introduced in Section II. The classification method is introduced in Section III. Simulation and real data experiment are in Section IV. Section V is the conclusion.

II. PIXEL-WISE H AND α

In SAR polarimetry, traditional method uses full aperture data to calculate H and α [12], because the aperture is small and polarimetric scattering properties are assumed invariant. When azimuthal view angle is large, changing polarimetric properties are no longer negligible and can affect the estimation of H and α. Targets of changing polarimetric properties along azimuth, i.e. anisotropic targets, need suitable method to calculate H and α. Firstly, MAPE is introduced and is used to identify anisotropic and isotropic targets.

A. IDENTIFY ANISOTROPIC AND ISOTROPIC TARGETS

The coherent scattering matrix $\boldsymbol{S}$ contains full polarimetric information about targets,

$$\boldsymbol{S} = \begin{bmatrix} S_{HH} & S_{HV} \\ S_{VH} & S_{VV} \end{bmatrix}, \tag{1}$$

where H and V represent horizontal and vertical polarization respectively. When the reciprocal backscattering case that $S_{HV} = S_{VH}$ is met, the target vector with Pauli base is defined as [16]

$$\boldsymbol{k} = \frac{1}{\sqrt{2}}[S_{HH} + S_{VV} \quad S_{HH} - S_{VV} \quad 2S_{HV}]^T, \tag{2}$$

where the operator ^{T} denotes transpose. Targets' polarimetric properties are assumed invariant within the synthetic aperture of traditional PolSAR. As to polarimetric CSAR, the synthetic aperture is much larger and polarimetric properties achieved from different angles of view are possibly different. Thus the observation procedure should be viewed as m times independent observation from m angles of view. Consequently polarimetric CSAR data are cut into m sub-apertures with equal size to obtain polarimetric information about m angles of view. In this case, target vectors from m sub-apertures are combined [11]:

$$\boldsymbol{p} = [\boldsymbol{k}_1^T \quad \boldsymbol{k}_2^T \cdots \boldsymbol{k}_m^T]^T. \tag{3}$$

$\boldsymbol{p}$ is the target vector for multi-aperture situation. The dimension of $\boldsymbol{p}$ is $l = 3m$. $\boldsymbol{p}$ contains full polarimetric information about m angles of view. The $l \times l$ n-look multi-aperture sample coherency matrix $\boldsymbol{D}$ is

$$\boldsymbol{D} = \frac{1}{n}\sum_{j=1}^{n} \boldsymbol{p_j} \cdot \boldsymbol{p_j}^{T*} = \begin{bmatrix} \boldsymbol{T}_{11} & \boldsymbol{T}_{12} & \cdots & \boldsymbol{T}_{1m} \\ \boldsymbol{T}_{21} & \boldsymbol{T}_{22} & \cdots & \boldsymbol{T}_{2m} \\ \vdots & & \ddots & \vdots \\ \boldsymbol{T}_{m1} & \cdots & & \boldsymbol{T}_{mm} \end{bmatrix}, \tag{4}$$

where the operator * denotes conjugate, $\boldsymbol{p_j}$ is the jth sample of multi-aperture target vector. n is the number of independent samples. n is recommended being larger than 49 (7×7 Boxcar filter) to avoid the effect of speckle [18], [19]. In the following experiment, n equals 81(9×9 Boxcar filter). $\boldsymbol{T}_{ii}$ is the sample coherency matrix of ith sub-apertures. $\boldsymbol{T}_{il}$ is the cross-correlation between target vectors of the

ith and lth sub-aperture. If the spectrum of ith and lth sub-aperture does not overlap, then the ith and lth sub-apertures do not have coherency and $\boldsymbol{T}_{il}$ does not have useful information [20], [11]. In this article, all sub-apertures are chosen to not overlap between each other in spectrum. Off-diagonal items in (4) are then forced to zero to eliminate the influence of useless information:

$$\boldsymbol{T}_{il} = \begin{cases} \frac{1}{n}\sum_{j=1}^{n} \boldsymbol{k}_{ij} \cdot \boldsymbol{k}_{lj}^{T*} & if\ i = l \quad i, l \in (1 \cdots m) \\ 0 & if\ i \neq l \quad i, l \in (1 \cdots m), \end{cases} \tag{5}$$

where $\boldsymbol{k}_{ij}$ is the target vector for the jth sample of the ith sub-aperture. Combining (4) and (5), $\boldsymbol{D}$ can be simplified to

$$\boldsymbol{D} = \begin{bmatrix} \boldsymbol{T}_{11} & 0 & \cdots & 0 \\ 0 & \boldsymbol{T}_{22} & \cdots & 0 \\ \vdots & & \ddots & \vdots \\ 0 & \cdots & & \boldsymbol{T}_{mm} \end{bmatrix}. \tag{6}$$

Applying eigen-decomposition to $\boldsymbol{D}$,

$$\begin{aligned} \boldsymbol{D} = \boldsymbol{U}_D \boldsymbol{\Sigma}_D \boldsymbol{U}_D^{-1} &= \begin{bmatrix} \boldsymbol{U}_{11}\boldsymbol{\Sigma}_{11}\boldsymbol{U}_{11}^{-1} & & \\ & \boldsymbol{U}_{22}\boldsymbol{\Sigma}_{22}\boldsymbol{U}_{22}^{-1} & \\ & & \ddots \\ & & \boldsymbol{U}_{mm}\boldsymbol{\Sigma}_{mm}\boldsymbol{U}_{mm}^{-1} \end{bmatrix} \\ &= \sum_{i=1}^{3m} \lambda_i \boldsymbol{u}_i \boldsymbol{u}_i^{T*} \\ with\ \boldsymbol{T}_{jj} &= \boldsymbol{U}_{jj}\boldsymbol{\Sigma}_{jj}\boldsymbol{U}_{jj}^{-1} \quad j \in (1 \cdots m), \end{aligned} \tag{7}$$

where $\boldsymbol{U}$ is composed of eigenvectors, $\boldsymbol{u}$; $\boldsymbol{\Sigma}$ is composed of eigenvalues, λ. The eigenvalues of $\boldsymbol{D}$ are the same as the eigenvalues of each sub-aperture. MAPE is defined as [11]:

$$\begin{aligned} H_{multi} &= -\sum_{k=1}^{3m} P_k \log_{3m}(P_k) \\ with\ P_k &= \frac{\lambda_k}{\sum_{i=1}^{3m} \lambda_i}, \end{aligned} \tag{8}$$

H_{multi} is the MAPE, extension of polarimetric entropy in multi-aperture situation. MAPE describes not only degree of polarimetric randomness, but also variations in sub-apertures. When MAPE equals 1, all eigenvalues are the same, which corresponds to isotropic targets of high polarimetric randomness. The case when MAPE equals 0 implies that only one eigenvalue is larger than 0, which corresponds to anisotropic point targets of no polarimetric randomness. Thus MAPE can be used to identify anisotropic and isotropic targets.

B. DETECT DOMINANT SCATTERING DIRECTION

Anisotropic targets have different scattering mechanisms in different sub-apertures. The scattering mechanisms of anisotropic targets are usually represented by one or a few sub-apertures corresponding to the dominant scattering direction. Sub-aperture(s) corresponding to the dominant scattering direction usually is or are highly different from other sub-apertures. Thus to acquire the scattering mechanism of anisotropic targets, the most different sub-aperture should be detected firstly. The target vector $\boldsymbol{k}$ is subject to multivariate complex Gaussian distribution [3], [21]:

$$p_{\boldsymbol{k}}(\boldsymbol{k}) = \frac{1}{\pi^3 |\boldsymbol{\Sigma}|} \exp(-\boldsymbol{k}^{T*} \boldsymbol{\Sigma}^{-1} \boldsymbol{k}). \tag{9}$$

The coherency matrix $\boldsymbol{\Sigma} = E\{\boldsymbol{k}\boldsymbol{k}^{T*}\}$. $|\boldsymbol{\Sigma}|$ denotes the determinant of $\boldsymbol{\Sigma}$. $E\{\boldsymbol{k}\boldsymbol{k}^{T*}\}$ denotes the expectation of $\boldsymbol{k}\boldsymbol{k}^{T*}$. The sample coherency matrix $\boldsymbol{T}$ is subject to complex Wishart distribution $W_C(n, \boldsymbol{\Sigma})$ [22]:

$$p(\boldsymbol{T}) = \frac{n^{3n} |\boldsymbol{T}|^{n-3} \exp[-n\mathrm{Tr}(\boldsymbol{\Sigma}^{-1}\boldsymbol{T})]}{|\boldsymbol{\Sigma}|^n K(n, 3)}. \tag{10}$$

$\mathrm{Tr}(\boldsymbol{\Sigma}^{-1}\boldsymbol{T})$ represents the trace of $\boldsymbol{\Sigma}^{-1}\boldsymbol{T}$.

$$K(n, 3) = \pi^3 \Gamma(n)\Gamma(n-1)\Gamma(n-2). \tag{11}$$

$\Gamma(\cdot)$ is Gamma function. This article uses maximum-likelihood ratio to detect the most different sub-aperture. The sample coherency matrix of m sub-apertures is $\boldsymbol{T}_{ii}$, with $i = 1, \ldots, m$. The m sample covariance matrices are tested for the following hypothesis [10]:

$$\begin{aligned} &\mathrm{H}_0 : \boldsymbol{\Sigma}_1 = \boldsymbol{\Sigma}_2 = \ldots = \boldsymbol{\Sigma}_m = \boldsymbol{\Sigma} \\ &\mathrm{H}_1 : \boldsymbol{\Sigma}_i = \boldsymbol{\Sigma}_A \neq \boldsymbol{\Sigma}_l = \boldsymbol{\Sigma}_B, i \in \boldsymbol{L}_A, l \in \boldsymbol{L}_B \\ &\boldsymbol{L}_A \cap \boldsymbol{L}_B = \emptyset, \end{aligned} \tag{12}$$

where $\boldsymbol{\Sigma}_i$ is the coherency matrix of ith sub-aperture. $\boldsymbol{L}_A$ and $\boldsymbol{L}_B$ are two different classes of sub-apertures. If H_0 is accepted, it means all the matrices belong to the same distribution and targets are isotropic. If H_1 is accepted, it means there are two different kinds of distribution and targets are anisotropic. The corresponding maximum-likelihood ratio Λ is

$$\Lambda = \left(\frac{|\boldsymbol{T}_A|^{M_A} |\boldsymbol{T}_B|^{M_B}}{|\widehat{\boldsymbol{T}}|^{M_T}}\right)^n, \tag{13}$$

with $M_T = M_A + M_B$, $\widehat{\boldsymbol{T}} = (M_A\boldsymbol{T}_A + M_B\boldsymbol{T}_B)/M_T$. M_A and M_B represents the total number of sub-apertures in class $\boldsymbol{L}_A$ and $\boldsymbol{L}_B$ respectively. $\boldsymbol{T}_A$ and $\boldsymbol{T}_B$ are defined as

$$\begin{aligned} \boldsymbol{T}_A &= \sum\nolimits_{i=1} \boldsymbol{T}_{ii}/M_A \quad i \in \boldsymbol{L}_A \\ \boldsymbol{T}_B &= \sum\nolimits_{l=1} \boldsymbol{T}_{ll}/M_B \quad l \in \boldsymbol{L}_B. \end{aligned} \tag{14}$$

The higher Λ is, the larger probability to accept H_0 is. The smaller Λ is, the larger probability to accept H_1 is. In this article, Λ is calculated m times. Each time the ith sub-aperture is selected as class $\boldsymbol{L}_A$ and the rest as class $\boldsymbol{L}_B$, where $i = 1, \ldots, m$. The sub-aperture corresponds to the smallest Λ is selected as the most different sub-aperture.

C. ALGORITHM

Traditional method to calculate H and α applies eigen-decomposition to sample coherency matrix of full aperture data. During the integration of sub-apertures, the scattering mechanisms of targets are in fact the average of all sub-apertures. Thus the integration of sub-apertures causes deviations when estimating H and α. To describe the scattering

properties precisely, this article proposes a pixel-wise method to calculate H and α.

1) Cut the polarimetric data into m sub-apertures. Consequently, m sub-aperture images are acquired.
2) Calculate the MAPE of each pixel.
3) Use MAPE to decide whether a pixel is anisotropic or isotropic. The boundary value is 0.5, which is a empirical value.
4) Use maximum likelihood ratio to find the most different sub-aperture of anisotropic pixels.
5) Use the sample coherency matrix which is from the most different sub-aperture to calculate H and α.
6) As to isotropic pixels, use the sample coherency matrix of full aperture data to calculate H and α.

Our method uses only data from the dominant direction to calculate anisotropic targets' H and α because scattering mechanisms in other directions are usually different. Then we use full aperture data to calculate isotropic targets' H and α because isotropic targets have same scattering mechanisms in all directions.

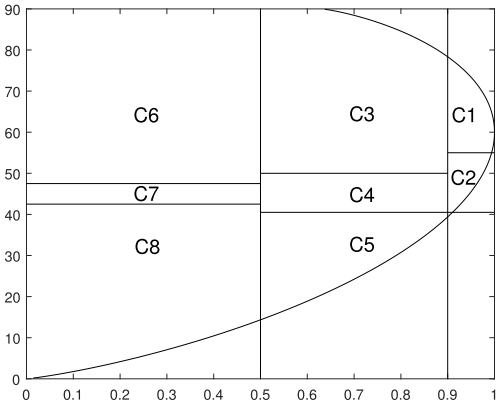

FIGURE 1. H/α classification plane [12].

TABLE 1. Classes in H/α classification [12].

Class	Class meaning
C1	High Entropy Multiple Scattering
C2	High Entropy Vegetation Scattering
C3	Medium Entropy Multiple Scattering
C4	Medium Entropy Vegetation Scattering
C5	Medium Entropy Surface Scatter
C6	Low Entropy Multiple Scattering Events
C7	Low Entropy Dipole Scattering
C8	Low Entropy Surface Scatter

III. CLASSIFICATION METHOD

A. PIXEL-WISE H/α AND MAPE CLASSIFICATION

Figure 1 shows the H/α classification plane and Table 1 shows the meanings of each class [12]. However, H/α plane can not distinguish anisotropic and isotropic targets which have same polarimetric scattering properties. In this article, the proposed classification method uses the pixel-wise H/α and MAPE as three dimensions to classify polarimetric CSAR data. The classification space is shown in Figure 2. Traditional H/α plane has 8 classes. Our pixel-wise H/α and MAPE classification method divides the 8 classes into 16 classes. Table 2 shows the meanings of each class.

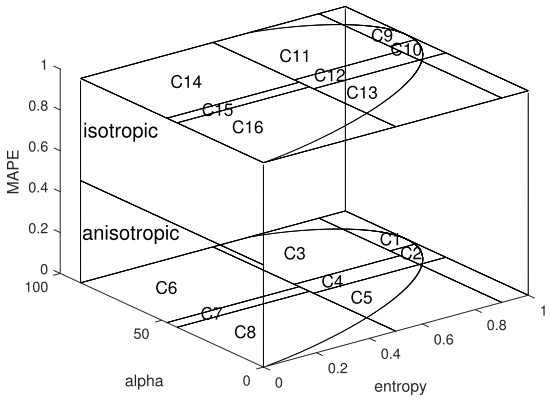

FIGURE 2. H/α/MAPE classification space.

TABLE 2. Classes in H/α/MAPE classification.

Class	Class meaning
C1	Anisotropic High Entropy Multiple Scattering
C2	Anisotropic High Entropy Vegetation Scattering
C3	Anisotropic Medium Entropy Multiple Scattering
C4	Anisotropic Medium Entropy Vegetation Scattering
C5	Anisotropic Medium Entropy Surface Scatter
C6	Anisotropic Low Entropy Multiple Scattering Events
C7	Anisotropic Low Entropy Dipole Scattering
C8	Anisotropic Low Entropy Surface Scatter
C9	Isotropic High Entropy Multiple Scattering
C10	Isotropic High Entropy Vegetation Scattering
C11	Isotropic Medium Entropy Multiple Scattering
C12	Isotropic Medium Entropy Vegetation Scattering
C13	Isotropic Medium Entropy Surface Scatter
C14	Isotropic Low Entropy Multiple Scattering Events
C15	Isotropic Low Entropy Dipole Scattering
C16	Isotropic Low Entropy Surface Scatter

The partition of the H/α slice is same as traditional H/α classification, as shown in [12]. The threshold of MAPE to determine whether targets are anisotropic or isotropic is 0.5. Pixel-wise H/α and MAPE method can more precisely classify anisotropic targets since H and α of anisotropic targets are estimated more precisely. Moreover, anisotropic and isotropic targets of same polarimetric scattering are classified into different classes in pixel-wise H/α and MAPE method. For instance, dihedral and top-hat both have dihedral scattering(when radar is facing dihedral directly) but one is anisotropic the other is isotropic. In pixel-wise H/α and MAPE method, dihedral will be in C6 and top-hat will be in C14.

Pixel-wise H/α and MAPE method has two problems. Firstly, C1, C2, C3, C4, and C5 refer to when MAPE is lower than 0.5 and pixel-wise entropy is larger than 0.5, which means targets are anisotropic but polarimetric randomness is high. When targets are anisotropic, it means

TABLE 3. Classes in MAPE/pixel-wise α classification.

Class	Class meaning
C1	Isotropic High Polarimetric Randomness Multiple Scattering
C2	Isotropic High Polarimetric Randomness Vegetation Scattering
C3	Isotropic Medium Polarimetric Randomness Multiple Scattering
C4	Isotropic Medium Polarimetric Randomness Vegetation Scattering
C5	Isotropic Medium Polarimetric Randomness Surface Scatter
C6	Isotropic Low Polarimetric Randomness Multiple Scattering Events
C7	Isotropic Low Polarimetric Randomness Dipole Scattering
C8	Isotropic Low Polarimetric Randomness Surface Scatter
C9	Anisotropic Low Polarimetric Randomness Multiple Scattering Events
C10	Anisotropic Low Polarimetric Randomness Dipole Scattering
C11	Anisotropic Low Polarimetric Randomness Surface Scatter

targets have dominant scattering directions and other sub-apertures usually have much lower power. Thus eigenvalues of the dominant sub-aperture(s) mainly determine the value of MAPE. Pixel-wise entropy of anisotropic targets is calculated with data from the dominant sub-aperture. MAPE is calculated from eigenvalues of all sub-apertures. Thus MAPE and entropy of anisotropic targets are very close. Sub-apertures which are not the dominant one usually have high polarimetric randomness and make MAPE higher than pixel-wise entropy. So the case when MAPE is lower than 0.5 and pixel-wise entropy larger than 0.5 should not exist. Secondly, MAPE is suggested as extension of polarimetric entropy in multi-observation situation in [11]. Since MAPE contains both polarimetric and angle information, it can not only be used to identify anisotropic and isotropic targets, but also distinguish targets of different polarimetric randomness. Thus pixel-wise entropy offers only redundant information. The two problems can be solved by further improvement.

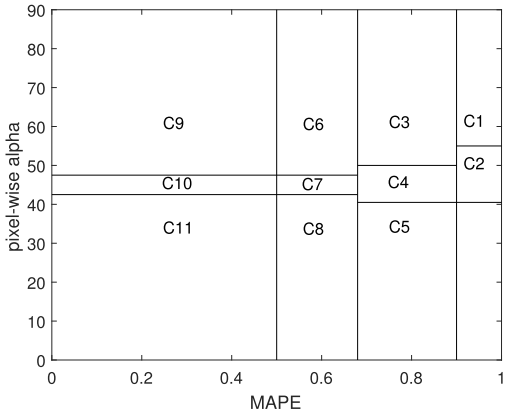

FIGURE 3. MAPE/pixel-wise α classification plane.

B. MAPE/PIXEL-WISE α CLASSIFICATION METHOD

MAPE and pixel-wise α classification method is an improved version of pixel-wise H/α and MAPE classification method. The method only has two classification features and 11 classes. The classification plane is shown in Fig. 3 and meanings of each class are shown in Table 3. The summary of each class is presented as follows:

1) C11: anisotropic low polarimetric randomness surface scatter
   This class is when MAPE is lower than 0.5 and pixel-wise α lower than 42.5°. This class contains anisotropic surface scattering such as Bragg-resonance over natural surface and the edge of the foot path.
2) C10: anisotropic low polarimetric randomness dipole scattering
   This class is when MAPE is lower than 0.5 and pixel-wise α between 42.5° and 47.5°. In this class, the amplitude of *HH* and *VV* has a large imbalance. Power lines are in this class.
3) C9: anisotropic low polarimetric randomness multiple scattering events
   This class is when MAPE is lower than 0.5 and pixel-wise α larger than 47.5°. This class contains dihedral scattering with low entropy, such as dihedral scatterers. Dihedral formed by wall and ground is in this class.
4) C8: isotropic low polarimetric randomness surface scatter
   This class is when MAPE is larger than 0.5 and lower than 0.68 together with pixel-wise α lower than 42.5°. This class contains isotropic surface scattering which has low polarimetric randomness. Sphere is in this class.
5) C7: isotropic low polarimetric randomness dipole scattering
   This class is when MAPE is larger than 0.5 and lower than 0.68 together with pixel-wise α larger than 42.5° and lower than 47.5°. This class contains isotropic dipole scattering which has low polarimetric randomness.
6) C6: isotropic low polarimetric randomness multiple scattering events
   This class is when MAPE is larger than 0.5 and lower than 0.68 together with pixel-wise α larger than 47.5°. This class contains isotropic dihedral scattering which has low polarimetric randomness. Top-hat is in this class.
7) C5: isotropic medium polarimetric randomness surface scatter
   This class is when MAPE is larger than 0.68 and lower than 0.9 together with pixel-wise α lower than 40.5°.

This class contains isotropic surface scattering with medium polarimetric randomness caused by changes in surface roughness and canopy propagation effects [12].

8) C4: isotropic medium polarimetric randomness vegetation scattering
   This class is when MAPE is larger than 0.68 and lower than 0.9 together with pixel-wise α larger than 40.5° and lower than 50.5°. This class contains isotropic dipole scattering with medium polarimetric randomness caused by central statistical distribution of orientation angle [12].
9) C3: isotropic medium polarimetric randomness multiple scattering
   This class is when MAPE is larger than 0.68 and lower than 0.9 together with pixel-wise α larger than 50.5°. This class contains isotropic dihedral scattering with medium entropy. Vegetation area with canopies is in this class.
10) C2: isotropic high polarimetric randomness vegetation scattering
    This class is when MAPE is larger than 0.9 and pixel-wise α larger than 40.5° and lower than 55°. This class contains cloud of short dipole. Vegetation surfaces and random noise are in this class.
11) C1: isotropic high entropy multiple scattering
    This class is when MAPE is larger than 0.9 and pixel-wise α larger than 55°. This class contains double bounce which is highly affected by canopies. Some forest area is in this class.

IV. EXPERIMENTS

A. SIMULATION OF TYPICAL ANISOTROPIC TARGETS

Polarimetric data of three typical anisotropic targets are simulated with Feko 7.0 to illuminate the difference between traditional α and pixel-wise α. Our simulation includes a dihedral, a plane and a dipole, as shown in Fig. 4. Dihedral is made up of two squares which are 1/3 meter in length. Plane is 10 meters in length and 0.5 meter in width. Dipole is 0.25 meter in length. The source of the simulation is plane wave of 45° elevation angle and azimuthal angle from 0° to 360° from far field. The frequency of the plane wave is 600MHz.

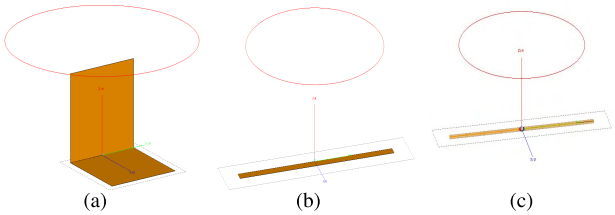

FIGURE 4. Simulation of (a) dihedral, (b) plane and (c) dipole.

The 360° scattering mechanisms of dihedral and plane is shown in Fig. 5(a) and 5(b). Freeman decomposition [23] is applied to determine the dominant scattering mechanisms

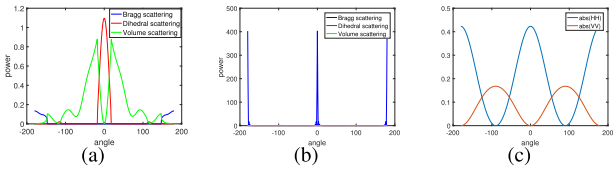

FIGURE 5. Freeman decomposition of (a) dihedral and (b) plane (blue: Bragg scattering; red: dihedral scattering; green: volume scattering). (c) The absolute value of dipole's *HH* and *VV* channel (blue: *HH* and red: *VV*).

from different angles of view. Dihedral and plane are anisotropic targets. In Fig. 5(c), the absolute values of dipole's *HH* and *VV* channel from different angles of view are used to represent dipole's scattering properties because Freeman decomposition does not contain dipole scattering. The dominant scatterings mechanisms of dihedral, plane and dipole are different when view angle changes. From −13° to 13° the dominant scattering mechanism of dihedral is dihedral scattering. Then from −13° to −147° and 13° to 147°, the dominant scattering mechanism is volume scattering. The dominant scattering mechanism in the rest part is Bragg scattering. Plane has Bragg scattering when view angle is from −8° to 8°. The rest part is dominant with volume scattering. When angle of view is 0°, the absolute value of dipole's *VV* channel is zero while in the rest part larger than zero. In these three cases, 0° is the dominant scattering direction and scattering from 0° can help us to understand the physical structure of the targets. Table 4 shows the traditional α and our proposed pixel-wise α of dihedral and plane. α is calculated with full aperture data whereas pixel-wise α is calculated with data from sub-aperture which starts from −2° to 2°. α of dihedral is 75.27, smaller than pixel-wise α because full aperture data combine scattering of all view angles and α of Bragg scattering is lower than 42.5. α of plane is 43.45, larger than pixel-wise α because full aperture data combine volume scattering and α of volume scattering is larger than 47.5. α of dipole is 45, equal pixel-wise α which means changes of angles of view hardly affects the calculation of dipole's α.

TABLE 4. α and pixel-wise α of dihedral and plane.

Targets	α	Pixel-wise α
dihedral	75.27	76.32
plane	43.45	26.05
dipole	45.0	45.0

According to the former discussion, α calculated with full aperture data are affected by scattering from all view angles, which can lower the precise of H/α classification result. Our proposed method calculates anisotropic targets' pixel-wise α with data from sub-aperture which is selected by maximum likelihood ratio. Targets' scattering properties are described more precisely by pixel-wise α. Meanwhile, pixel-wise H is

TABLE 5. Experimental parameters [2].

Polarization	HH HV VH VV
Carrier frequency	600 MHz
Bandwidth	200MHz
Circle Radius	≈3000 m
Mean height	≈3000 m

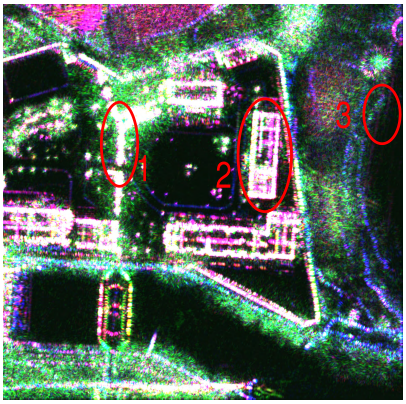

FIGURE 6. Full aperture using Pauli basis (blue: $|HH + VV|$; red: $|HH - VV|$; green: 2 $|HV|$).

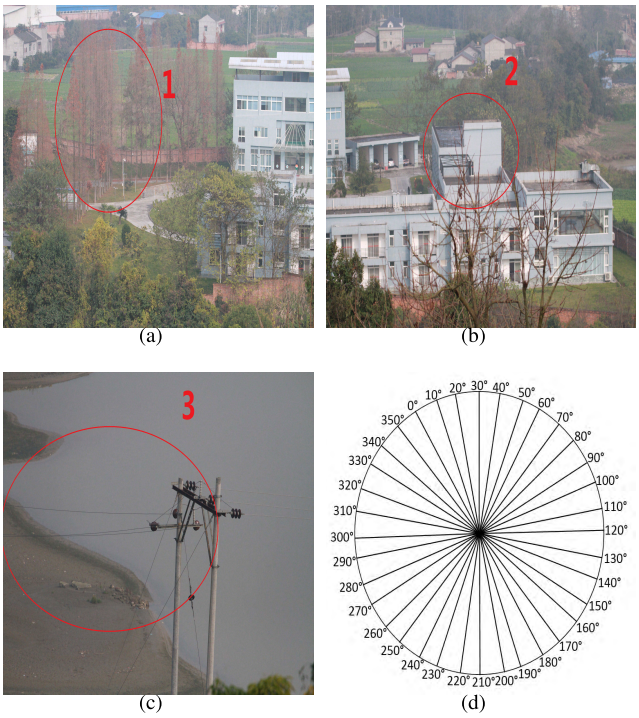

FIGURE 7. Optical image of (a) target 1, (b) target 2, (c) target 3 and (d) directions of sub-apertures.

FIGURE 8. Optical image of experimental scene.

also better than H calculated from full aperture data which is demonstrated by the following experiment on real data.

B. INFORMATION OF EXPERIMENTAL REAL DATA

The polarimetric CSAR data were acquired at Sichuan, China by P-band airborne CSAR system, Institute of Electronics, Chinese Academy of Sciences [2]. The imaging algorithm is back-projection algorithm. Data are polarimetric calibrated. The experimental parameters are shown in Table 5. The experimental area is shown in Fig. 6 and mainly contains a power station and some buildings. The local incidence angle of the experimental area is about 45°. Figure 8 is the optical image of experimental scene. The imaging scene center is to the center of Fig. 8. Three targets are selected. Target 1 is tall trees in the shape of capital Y. Target 2 is a building. Target 3 is power lines over a river. Three targets are shown in Fig. 7.

C. PIXEL-WISE H AND α

To acquire targets' scattering properties from different directions, polarimetric CSAR data are cut into 36 sub-apertures, each sub-aperture is 10° and do not overlap with each other in spectrum. The direction of each sub-aperture is shown in Fig. 7(d). Firstly, anisotropic targets identified by MAPE and their directions calculated by maximum likelihood ratio are shown in Fig. 9. When MAPE is lower than 0.5, targets are anisotropic. Target 1 is not in Fig. 9 because trees are isotropic. Four walls of target 2 form dihedrals with ground. According to the former discussion, the dominant direction of dihedral is when sensor is facing it directly. Thus target 2 has 4 colors, corresponding to 70°, 150°, 230° and 330°. The walls of target 2 do not exactly face only one sub-aperture. Thus the directions of four walls may have a 10° deviation. Consequently the angles between the four directions do not exactly equal 90°. Power lines have dipole scattering when the view angle of sensor is vertical to them. Thus power lines actually have two scattering directions. In our method, only one scattering direction is picked up, depends on which direction has smaller Λ. In Fig. 9, target 3 has two colors, which refer to 150° and 340°. The corresponding sub-apertures are close to the vertical directions of the power lines.

Figure 10(a) and Fig. 10(c) shows the polarimetric entropy and α. Figure 10(b) and Fig. 10(d) shows the pixel-wise H and α. In our proposed method, H and α of isotropic targets are calculated based on full aperture data whereas anisotropic

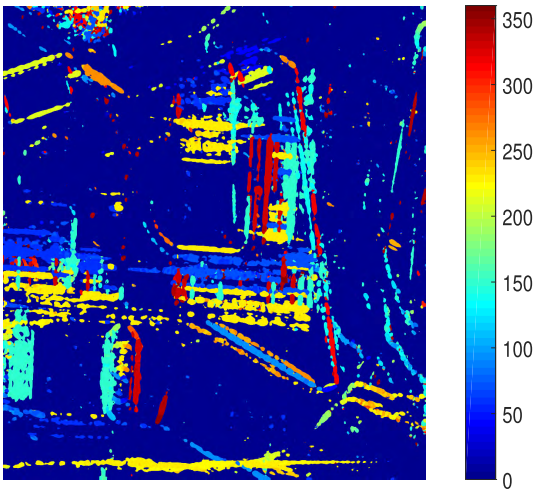

FIGURE 9. Anisotropic targets and their dominant directions.

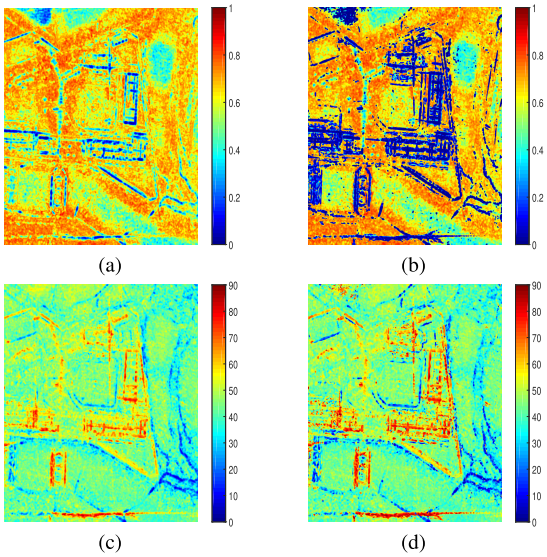

FIGURE 10. (a) Polarimetric entropy, (b) pixel-wise calculated polarimetric entropy, (c) α and (d) pixel-wise calculated α.

targets' H and α are calculated based on data of the sub-aperture selected by maximum likelihood ratio. Thus the difference between Fig. 10(a), 10(c) and Fig. 10(b), 10(d) is caused by anisotropic targets. Figure 11(a) and 11(b) show the histogram of difference between traditional and pixel-wise H and α. Anisotropic targets have low polarimetric randomness when sensor is facing their dominant scattering directions whereas have high polarimetric randomness when sensor is not facing their dominant scattering directions. During the formation of full apertures, the polarimetric randomness becomes higher compared to when sensor is facing the dominant scattering direction. Thus anisotropic targets' pixel-wise polarimetric entropy is lower than polarimetric entropy. The changes of α are more complex. The pixel-wise α for anisotropic targets of dihedral scattering is larger

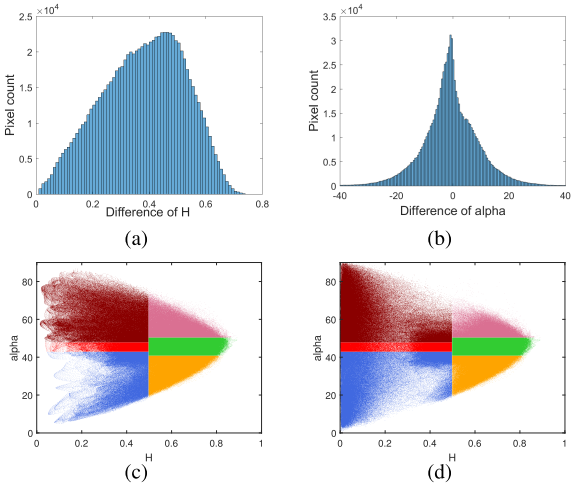

FIGURE 11. The histogram of (a) polarimetric entropy difference and (b) α difference, together with distribution of (c) H-α and (d) pixel-wise calculated H-α of Fig. 6.

than traditional α. The pixel-wise α for anisotropic targets of Bragg scattering is smaller than traditional α. The result is same with our former simulation. Figure 11(c) and 11(d) show the distribution of traditional and pixel-wise H and α on classification plane. In Fig. 11(d), anisotropic targets have lower H. Also the distance between α of anisotropic targets and the classification boundary is larger. Thus our proposed method can improve the precision of classification result.

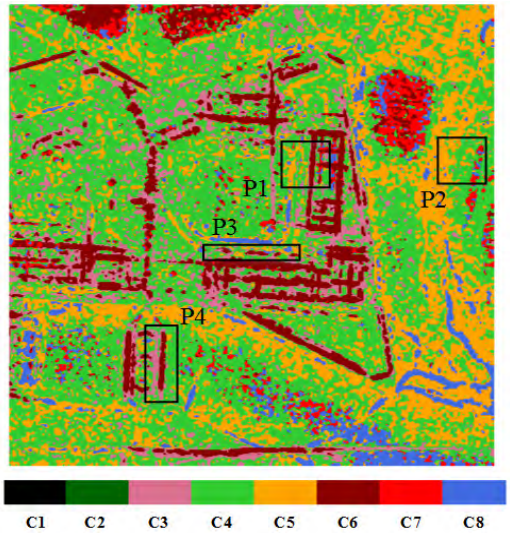

FIGURE 12. H/α classification result.

The H/α classification and pixel-wise H/α classification results are shown in Fig. 12 and 13, respectively. Four parts in the scene are selected to illuminate the difference between two classification results. P1 and P3 are part of the footpath, which has Bragg scattering and should be C8 in H/α classification. However, the right line of the foot path is C5, because

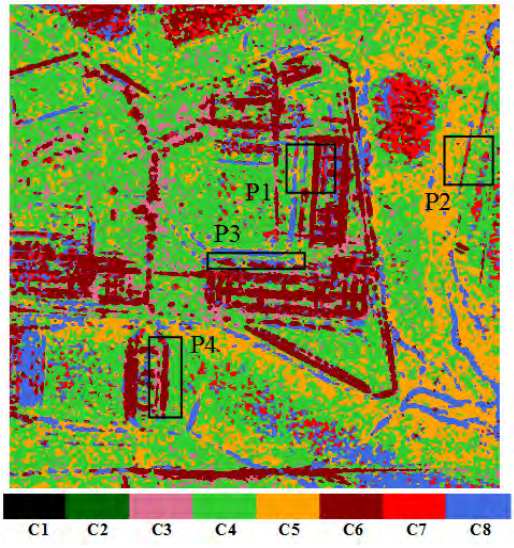

FIGURE 13. Pixel-wise H/α classification result.

H is overestimated. In Fig. 13, the result shows that H is calculated correctly with our proposed method and footpath is correctly classified as C8. P2 is power lines which have dipole scattering and should be C7 in H/α classification. However, in Fig. 12, a part of the power lines is C4, also because entropy is overestimated. P4 is a bridge, which has dihedral scattering and should be C6 in H/α classification. In Fig. 12, a part of the bridge is C3 because entropy is overestimated. In Fig. 13, the entropy of P2 and P4 are correctly calculated. Power lines and bridge are correctly classified.

D. PIXEL-WISE H/α AND MAPE CLASSIFICATION

Although H and α are correctly calculated, the classification result is not precise enough. In Fig.13, target 1 and target 2 is classified as C6, dihedral scattering which means they are hard to distinguish with polarimetric information. However, trees are isotropic targets and buildings are anisotropic targets. Target 1 and target 2 can be distinguished with azimuth information. H/α/MAPE classification space is applied to acquire more precise classification result. Figure 14 is the pixel-wise H/α and MAPE classification result. If MAPE is lower than 0.5, targets are considered as anisotropic and higher than 0.5, isotropic. Target 1 and target 2 are classified into two classes by H/α/MAPE classification method, as shown in Fig. 14. Target 1 is classified as C14, isotropic dihedral scattering while target 2 is classified as C6, anisotropic dihedral scattering. Target 3 is classified as C7, anisotropic dipole scattering. Bridge is C6, anisotropic dihedral scattering while the footpath is C8, anisotropic Bragg scattering. Ground and river surface which is C4 in Fig. 12 is classified as C12 in Fig. 14. The classification result fits in with our expectation. The result shows the proposed classification method can distinguish anisotropic and isotropic targets which have same polarimetric scattering properties.

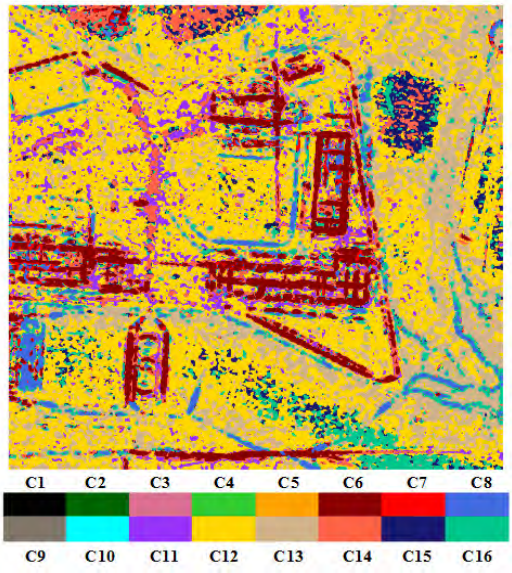

FIGURE 14. H/α/MAPE classification result.

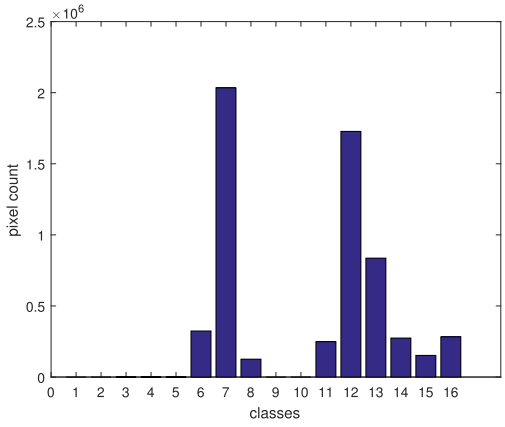

FIGURE 15. Pixel count of each class.

Still the classification result has some problems. Figure 15 shows the pixel count of each class defined in pixel-wise H/α and MAPE classification. Anisotropic targets can hardly have high polarimetric entropy, which means when targets' MAPE is lower than 0.5, targets' entropy is hardly higher than 0.5. Thus there are few pixels which fall into C1, C2, C3, C4, and C5. There are few pixels falling into C9 and C10 too, but this is because targets of high entropy multiple scattering and high entropy vegetation scattering are naturally rare. The histogram of pixel-wise H/α and MAPE classification result demonstrates our former discussion.

E. MAPE/PIXEL-WISE α CLASSIFICATION

The classification result of our further improved classification method is shown in Fig. 16. The colors of each class defined in MAPE/pixel-wise α classification are same with the colors in H/α/MAPE classification for better comparison. Firstly, the results shown in Fig. 16 are almost same

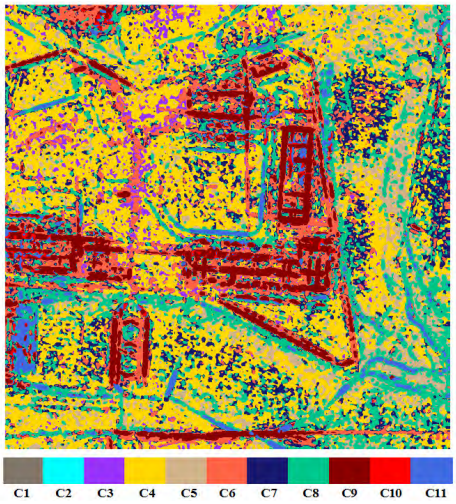

FIGURE 16. MAPE/pixel-wise α classification result.

with results shown in Fig. 14, which suggests the classification results are correct even if the classification dimensions reduce from 3 to 2. The improvement is significant since MAPE/pixel-wise α classification method is less complex and has almost same result as pixel-wise H/α and MAPE method.

V. CONCLUSION

In this paper, pixel-wise H/α calculation method to eliminate the deviations caused by anisotropic scattering is proposed. Firstly, polarimetric CSAR data are cut into sub-apertures. MAPE is then introduced and used to identify anisotropic and isotropic targets. The dominant scattering directions of anisotropic targets are then detected by maximum likelihood ratio and consequently the corresponding sub-aperture is selected. H and α of anisotropic targets are calculated based on data from the sub-aperture which is corresponding to dominant direction. H and α of isotropic targets are calculated based of full aperture data. Our pixel-wise H and α avoid the affection of scatterings which are not from the dominant direction. The values of pixel-wise H and α are more accurate and can improve the precision of H/α classification result. The effectiveness of our proposed method is demonstrated by both simulation and real data experiment.

An unsupervised classification method is proposed. The proposed method uses MAPE and pixel-wise H/α as three dimensions to create a classification space. The initial 8 classes defined by H/α plane then increase to 16 classes. Also the classification plane becomes a classification space. With the proposed method, anisotropic and isotropic targets which have same polarimetric scattering properties can be distinguished. In real data experiment, typical targets which are correctly classified by H/α plane are also correctly classified by H/α/MAPE space. Moreover, trees and buildings, which both have dihedral scattering(when sensor is facing the walls of the building directly), are also distinguished by H/α/MAPE space. Trees are classified as isotropic dihedral scattering and buildings are classified as anisotropic dihedral scattering.

The method is then further improved. Five classes are removed because they do not exist on real world. In addition, since MAPE can also describe polarimetric randomness, pixel-wise entropy is replaced by MAPE. Consequently the classification space degenerate into a plane. The meaning of each class and corresponding typical targets are discussed. In real data experiment, the further improved method has almost the same result as the original one. Moreover the affection of volume scattering in tree area is reduced in the improved method.

Although the research topic is polarimetric CSAR in this article, our proposed pixel-wise H and α and unsupervised classification method can also be applied to other polarimetric SAR data with anisotropic scattering.

REFERENCES

[1] O. Ponce *et al.*, "Fully polarimetric high-resolution 3-D imaging with circular SAR at L-Band," *IEEE Trans. Geosci. Remote Sens.*, vol. 52, no. 6, pp. 3074–3090, Jun. 2014.

[2] Y. Lin, W. Hong, W. Tan, Y. Wang, and Y. Wang, "Airborne circular SAR imaging: Results at P-band," in *Proc. IEEE Int. Geosci. Remote Sens. Symp.*, Jul. 2012, pp. 5594–5597.

[3] L. Ferro-Famil, A. Reigber, E. Pottier, and W. M. Boerner, "Scene characterization using subaperture polarimetric SAR data," *IEEE Trans. Geosci. Remote Sens.*, vol. 41, no. 10, pp. 2264–2276, Oct. 2003.

[4] L. R. Flake, S. C. Ahalt, and A. K. Krishnamurthy, "Detecting anisotropic scattering with hidden Markov models," *IEE Proc.-Radar, Sonar Navigat.*, vol. 144, no. 2, pp. 81–86, Apr. 1997.

[5] P. Runkle, L. H. Nguyen, J. H. McClellan, and L. Carin, "Multi-aspect target detection for SAR imagery using hidden Markov models," *IEEE Trans. Geosci. Remote Sens.*, vol. 39, no. 1, pp. 46–55, Jan. 2001.

[6] Y. Zhao, Y. Lin, W. Hong, and L. Yu, "Adaptive imaging of anisotropic target based on circular-SAR," *Electron. Lett.*, vol. 52, no. 16, pp. 1406–1408, 2016.

[7] F. Xu, Y. Li, and Y.-Q. Jin, "Polarimetric-anisotropic decomposition and anisotropic entropies of high-resolution SAR images," *IEEE Trans. Geosci. Remote Sens.*, vol. 54, no. 9, pp. 5467–5482, Sep. 2016.

[8] Y. Li, H. Wang, H. Zhang, and F. Xu, "Anisotropic analysis of polarimetric scattering and case studies with UAVSAR images," *Int. J. Remote Sens.*, vol. 37, no. 21, pp. 5176–5195, 2016.

[9] R. L. Moses, L. C. Potter, and M. Cetin, "Wide-angle SAR imaging," *Proc. SPIE*, vol. 5427, pp. 164–175, Sep. 2004.

[10] Y. Li, Y. Lin, J.-J. Zhang, X.-Y. Guo, S.-Q. Chen, and W. Hong, "Estimation and removing of anisotropic scattering for multiaspect polarimetric SAR image," *J. Radars*, vol. 4, no. 3, pp. 254–264, 2015.

[11] F. Xue *et al.*, "Analysis of azimuthal variations using multi-aperture polarimetric entropy with circular SAR images," *Remote Sens.*, vol. 10, no. 1, p. 123, 2018. [Online]. Available: http://www.mdpi.com/2072-4292/10/1/123

[12] S. R. Cloude and E. Pottier, "An entropy based classification scheme for land applications of polarimetric SAR," *IEEE Trans. Geosci. Remote Sens.*, vol. 35, no. 1, pp. 68–78, Jan. 1997.

[13] C. Lopez-Martinez, E. Pottier, and S. R. Cloude, "Statistical assessment of eigenvector-based target decomposition theorems in radar polarimetry," *IEEE Trans. Geosci. Remote Sens.*, vol. 43, no. 9, pp. 2058–2074, Sep. 2005.

[14] L. Ferro-Famil, E. Pottier, and J.-S. Lee, "Unsupervised classification of multifrequency and fully polarimetric SAR images based on the H/A/Alpha-Wishart classifier," *IEEE Trans. Geosci. Remote Sens.*, vol. 39, no. 11, pp. 2332–2342, Nov. 2001.

[15] J. S. Lee, M. R. Grunes, and R. Kwok, "Classification of multi-look polarimetric SAR imagery based on complex Wishart distribution," *Int. J. Remote Sens.*, vol. 15, no. 11, pp. 2299–2311, Jul. 1994.

[16] J.-S. Lee, M. R. Grunes, T. L. Ainsworth, L.-J. Du, D. L. Schuler, and S. R. Cloude, "Unsupervised classification using polarimetric decomposition and the complex Wishart classifier," *IEEE Trans. Geosci. Remote Sens.*, vol. 37, no. 5, pp. 2249–2258, Sep. 1999.
[17] E. Pottier, "Radar target decomposition theorems and unsupervized classification of full polarimetric SAR data," in *Proc. Surf. Atmos. Remote Sens., Technol., Data Anal. Interpretation Geosci. Remote Sens. Symp. (IGARSS)*, Aug. 1994, pp. 1139–1141.
[18] J. S. Lee, T. L. Ainsworth, J. P. Kelly, and C. Lopez-Martinez, "Evaluation and bias removal of multilook effect on entropy/alpha/anisotropy in polarimetric SAR decomposition," *IEEE Trans. Geosci. Remote Sens.*, vol. 46, no. 10, pp. 3039–3052, Oct. 2008.
[19] J.-S. Lee, T. L. Ainsworth, J. Kelly, and C. Lopez-Martinez, "Statistical evaluation and bias removal of multi-look effect on entropy/alpha/anisotropy in polarimetric target decomposition," in *Proc. Eur. Conf. Synth. Aperture Radar*, Jun. 2008, pp. 1–4.
[20] F. Gatelli, A. M. Guamieri, F. Parizzi, P. Pasquali, C. Prati, and F. Rocca, "The wavenumber shift in SAR interferometry," *IEEE Trans. Geosci. Remote Sens.*, vol. 29, no. 4, pp. 855–865, Jul. 1994.
[21] A. Alonso-Gonzalez, C. Lopez-Martinez, and P. Salembier, "Filtering and segmentation of polarimetric SAR data based on binary partition trees," *IEEE Trans. Geosci. & Remote Sens.*, vol. 50, no. 2, pp. 593–605, Feb. 2012.
[22] J.-S. Lee, K. W. Hoppel, S. A. Mango, and A. R. Miller, "Intensity and phase statistics of multilook polarimetric and interferometric SAR imagery," *IEEE Trans. Geosci. Remote Sens.*, vol. 32, no. 5, pp. 1017–1028, Sep. 1994.
[23] A. Freeman and S. L. Durden, "A three-component scattering model for polarimetric SAR data," *IEEE Trans. Geosci. Remote Sens.*, vol. 36, no. 3, pp. 963–973, May 1998.

FEITENG XUE (S'16) was born in Ganzhou, China, in 1995. He received the B.S. degree in electronic engineering from the University of Science and Technology of China in 2014. He is currently pursuing the Ph.D. degree in signal processing with the Institute of Electronics, Chinese Academy of Sciences, University of Chinese Academy of Sciences, Beijing, China.

His current interests are multi-aspect polarimetric synthetic aperture radar and anisotropic polarimetric scattering.

YUN LIN (M'16) received the B.S. degree from the Beijing University of Posts and Telecommunications in 2006 and the Ph.D. degree from the Institute of Electronics, Chinese Academy of Sciences, Beijing, China, in 2011.

She is currently an Associate Professor with the Institute of Electronics, Chinese Academy of Sciences, University of Chinese Academy of Sciences. Her current interests are circular synthetic aperture radar imaging and anisotropic scattering detection.

WEN HONG (M'03) was born in Xi'an, China, in 1968. She received the Ph.D. degree from the Beijing University of Aeronautics and Astronautics (BUAA), Beijing, China, in 1997.

She was a Faculty Member in signal and information processing with the Department of Electrical Engineering, BUAA, from 1997 to 2002. She was a Guest Scientist with DLR-HF, Wessling, Germany, from 1998 to 1999. Since 2002, she has been a Scientist with the Science and Technology on Microwave Imaging Laboratory, Institute of Electronics, Chinese Academy of Sciences, Beijing. Her research interests include polarimetric/polarimetric interferometric synthetic aperture radar (SAR) data processing and application, 3-D SAR signal processing, circular SAR signal processing, and sparse microwave imaging with compressed sensing.

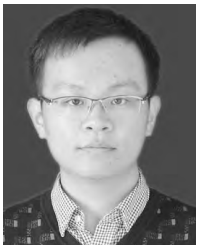

SHIQIANG CHEN (S'16) received the B.S. degree in electronics and information engineering from the University of Electronic Science and Technology of China, Chengdu, China, in 2013. He is currently pursuing the Ph.D. degree in information and signal processing with the Institute of Electronics, Chinese Academy of Sciences, University of Chinese Academy of Sciences, Beijing, China.

His research interests include investigations in compact polarimetry applications, system design, and analysis with the hybrid-polarity architecture-based polarimetric synthetic aperture radar system.

WENJIE SHEN (S'16) received the B.S. degree in electronic engineering from Shanxi University, China, in 2014, and the M.S. degree in signal and information processing from the Institute of Electronics, Chinese Academy of Sciences, University of Chinese Academy of Sciences, Beijing, China, in 2017, where he is currently pursuing the Ph.D. degree in signal and information processing.

His research interests include circular synthetic aperture radar (SAR) image formation and circular SAR GMTI.